Electronic Supplementary Information (ESI)

Phase selective synthesis of nickel silicide nanocrystals in molten salts for electrocatalysis of the oxygen evolution reaction

Ram Kumar,[a] Mounib Bahri,[b] Yang Song,[a] Francisco Gonell,[a] Cyril Thomas,[c] Ovidiu Ersen,[b] Clément Sanchez,[a] Christel Laberty-Robert,[a] David Portehault[a,*]

[a.] *Sorbonne Université, CNRS, Collège de France, Laboratoire de Chimie de la Matière Condensée de Paris (CMCP), 4 place Jussieu, F-75005, Paris, France.*

[b.] *Université de Strasbourg, CNRS, Institut de physique et de chimie des Matériaux de Strasbourg (IPCMS), 23 rue du Loess, 67200 Strasbourg, France.*

[c.] *Sorbonne Université, CNRS, Laboratoire de Réactivité de la Surface (LRS), 4 place Jussieu, F-75005, Paris, France*

Experimental methods:

Reagents and precursors: All chemicals were obtained from commercial sources (Sigma Aldrich, Alfa Aesar). Commercial reference IrO_2 nanoparticles for the electrochemical measurements were obtained from Alfa Aesar. The anhydrous LiI and KI salts were further dried at 300 °C for 2 days before the synthesis. All synthesis and manipulations were performed into a glovebox and under argon.

Synthesis of *Zintl*-Na_4Si_4: The ionic solid silicon precursor Na_4Si_4 was synthesized by following a modified procedure[1] of Kauzlarich *et al.*[2] Silicon (~ 325 meshes, 99%, Sigma-Aldrich) and NaH (95%, Sigma-Aldrich) powders were were mixed in a Si:NaH = 1:2.1 mol. ratio and ball milled for 4 min at 20 Hz (Retsch MM400 ball mill airtight stainless steel bowls of 50 mL, one steel ball of 62.3 g with diameter of 23 mm). The resulting mixture was transferred to a *h*-BN crucible covered with a lid and inserted into a quartz tube. The reaction was performed at 420 °C for 90 h in a vertical furnace under argon flow. After cooling down, the reaction medium was obtained as a two-sided pellet, the bottom part being brown-black and the top part being white. This white residue is made of the side-product NaOH and was carefully scratched away. The blackish pellet was grinded into a fine powder. XRD and solid-state NMR[1] confirmed that the material was made of Na_4Si_4. The yield was 93% versus the Si reagent.

Syntheses of NiSi: In a typical batch, Na_4Si_4 (0.375 mmol), $NiCl_2$ (1.05 mmol) and the LiI-KI eutectic mixture (24 mmol, 3.5 g, 0.63 mol% LiI and 0.37 mol% KI) were mixed by ball milling for 2 min at 20 Hz (Retsch MM400 ball mill airtight stainless steel bowls of 50 mL, one steel ball of 62.3 g with diameter of 23 mm). The mixture was transferred to a carbon crucible inserted into a quartz tube. The reaction was performed at 500 °C for 2.5 h in a vertical furnace under constant argon flow with a heating rate of 10 °C min^{-1}. After cooling down, the salts were washed away with a 0.01M HCl solution by washing at least six times and then dried under vacuum overnight at 50 °C. Note that if the starting Na_4Si_4 powder contained minor amounts of crystalline elemental silicon, this impurity was recovered in the final NiSi product. Hence, only the reactive Zintl phase Na_4Si_4 participated in the reaction. If Si is present in the crude NiSi product, this impurity can be eliminated by stirring the powder for 2 h in 2 mol L^{-1} NaOH, in which nickel silicides are stable. The yield was 91% versus the Ni reagent.

Synthesis of Ni_2Si: In a typical batch, Na_4Si_4 (0.375 mmol), $NiCl_2$ (2.85 mmol) and the LiI-KI eutectic mixture (30 mmol, 4.376 g) were used. The reactions were performed at 300 °C for 30 min under constant Ar flow and a heating rate of 10 °C min^{-1} . All other procedures were the same as for the NiSi synthesis. The yield was 57% based on Ni.

Instrumentation and materials characterization: Powder X-ray diffraction (XRD) was recorded using a Bruker D8 Discover diffractometer with Cu $K\alpha$ radiation. XRD and electron diffraction patterns were indexed along the 95448-ICSD and 646563-ICSD, 197775- ICSD references from the PDF-4 database for NiSi and Ni_2Si, respectively. Transmission electron microscopy and elemental mapping were performed using a JEOL 2100F microscope at an accelerating voltage of 200 kV. XPS spectra were recorded on an Omicron spectrometer using an Al $K\alpha$ source (1486.7 eV) as the source energy. The binding energies were referenced versus the aliphatic C1s peak (284.8 eV). Nitrogen adsorption-desorption isotherms were obtained at 77 K using BELSORB-max. The samples were degassed at 180 °C (3 °C/min) for 16 h before the measurement. Electrochemical measurements were performed on Bio-Logic potentiostat.

Electrochemical measurements: The electrochemical measurements were performed on a VPS Biologic potentiostat by employing a glassy carbon (GC) rotating disk electrode (RDE, Radiometer analytical) with a disk surface area of 0.07 cm^2. A three electrode setup was used with the catalyst coated GC working electrode, a platinum wire as the counter electrode and Ag/AgCl/Sat. KCl as the reference electrode. All measured potential were converted to the reversible hydrogen electrode RHE using $E_{Ag/AgCl}$ = 0.197 V/SHE and pH = 13. The working electrodes were prepared by polishing the GC surface with diamond (1 μm) and alumina (0.05 μm) pastes to reach mirror grade. Catalyst inks were prepared from the electrocatalyst powder, Acetylene Black (AB, Alfa Aesar) (99.9+ %, ~75 m^2/g) and Nafion-117 solution (5% in aliphatic alcohol, Sigma-Aldrich). The acetylene black powder was mildly functionalized with carboxylate groups to enhance the alcoholic dispersion by treating it in nitric acid.[3] Acetylene black (500 mg) was stirred overnight in 50 mL of HNO_3 (20%) at 80 °C, washed with water and dried under vacuum. The catalyst inks were prepared by dispersing 7 mg of catalyst powder in 5 mL of ethanol (99%), along with 5 mg of treated AB. The mixture was sonicated in a water bath for 2 h to obtain a uniform dispersion. The Nafion solution (220 μL) was subsequently added and again sonicated for another 20 min. The resulting dispersion was stable and aggregate free for at least 1 week. 2 μL of the catalyst ink was deposited on the GC substrate and dried in air for 30 min before measurement. The effective electrocatalyst loading was approximately 40 μg cm^{-2}_{disk}. The OER activity was measured in a O_2-saturated 0.1 M KOH with a rotating disk speed of 1600 rpm and a scan rate of 10 mV s^{-1}. The measurements were repeated at least twice with different electrodes to confirm the consistency of the data. Commercial reference IrO_2 nanoparticles for comparison was obtained from Alfa aesar (43396 reference number, diameter ranging between 20 and 100 nm). Note that Commercial IrO_2 200-400 nm long nanowires supplied by Aldrich (206237 reference number) and used in some previous reports yielded very low OER activity much lower than the nickel silicide particles we report herein. We have not considered this material to benchmark nickel silice nanomaterials.

Electrochemical impedance spectra (EIS) were recorded at the open circuit voltage (OCV, ~146.9 mV) of the electrode, employing an AC perturbation of 10 mV_{rms} in the frequency range from 50 kHz to 1 Hz. The resistance of the solution R_s was obtained from the resulting Nyquist plot and used for ohmic drop correction $E = E_m - iR_s$, where E is the corrected potential and E_m is the measured potential. The long term performance and stability of the NiSi catalyst was evaluated employing chronopotentiometry at a current density of 5 mA cm^{-2}_{disk} in O_2-saturated 0.1 M KOH electrolyte and rotating speed of 1600 rpm. An optimum 5 mA cm^{-2}_{disk} current density was selected for the stability test to avoid mechanical breakage of the composite electrode film by O_2 bubbles evolving at higher current density. The electrocatalyst sample was examined after chronopotentiometry by XPS and TEM.

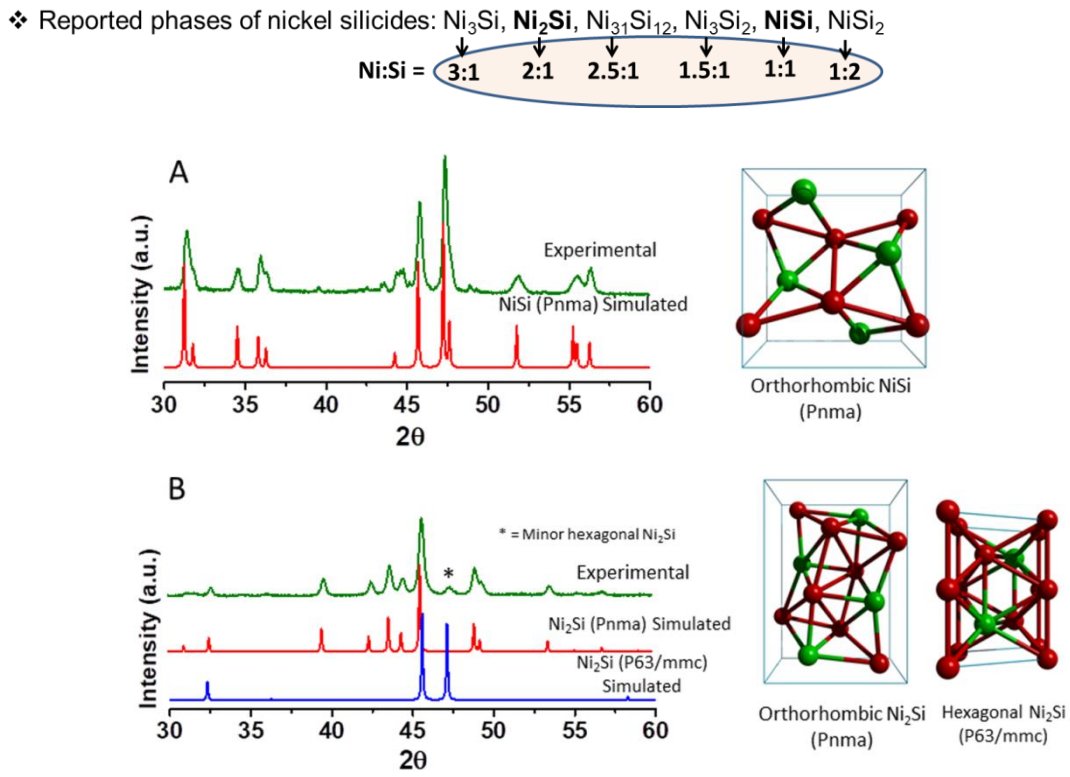

Fig. S1 Powder X-ray diffraction patterns of (A) NiSi and (B) Ni_2Si compared with the simulated patterns of the corresponding phases. Red ball = Ni and green ball = Si in the nickel silicide structures. NiSi orthorhombic P*nma* (62) (a = 5.17Å, b = 3.33Å, c = 5.6Å), Ni_2Si major orthorhombic P*nma* (62) (a = 4.97Å, b = 3.75Å, c = 7.06Å), Ni_2Si minor hexagonal P*63/mmc* (194) (a = 3.85 Å, c = 4.95).

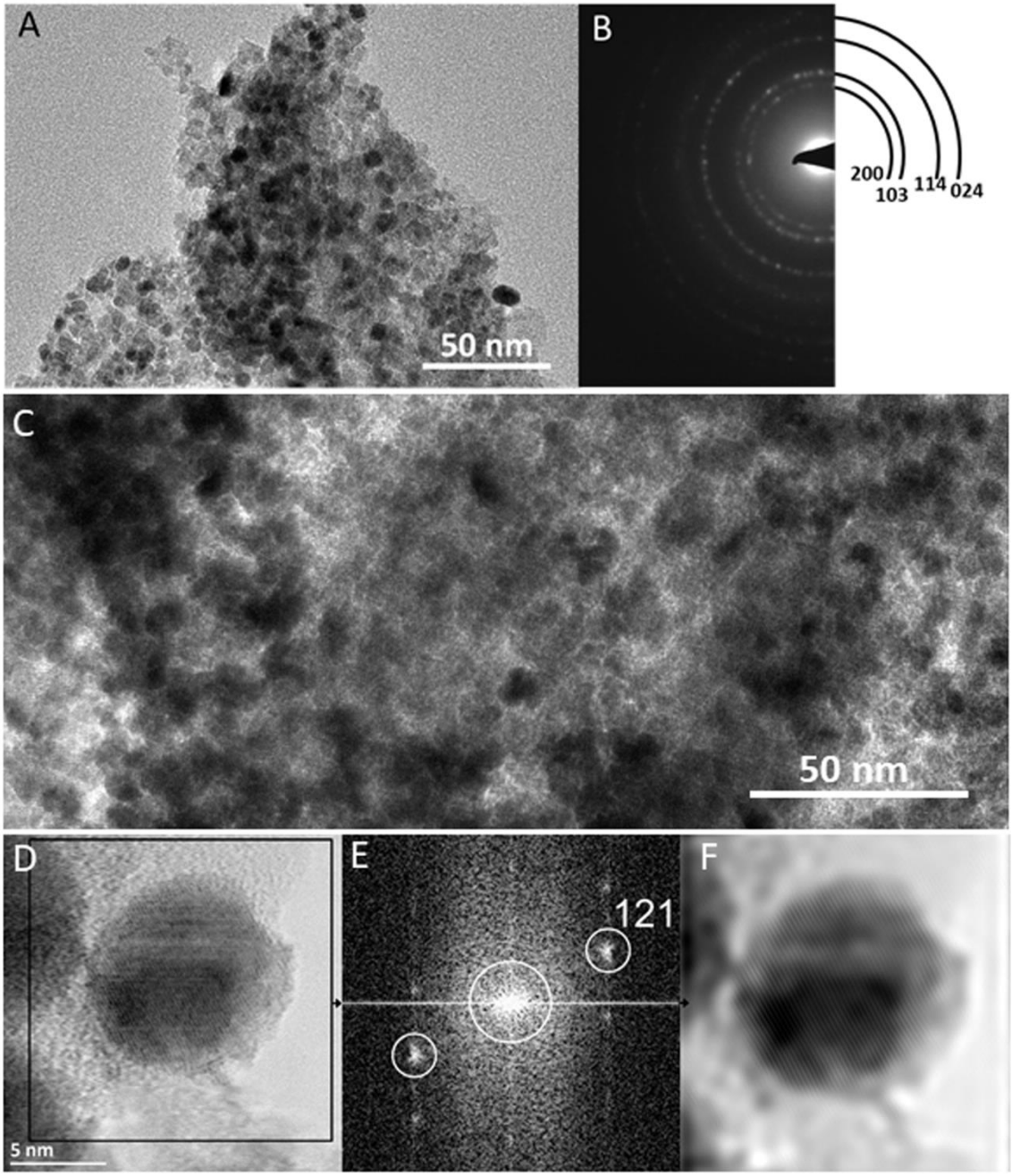

Fig. S2 (A, C) TEM image and (B) selected area electron diffraction (SAED) of Ni_2Si nanocrystals. (D) High-resolution HRTEM showing a Ni_2Si nanocrystal. (E) Corresponding FFT indexed along the o-Ni_2Si structure and showing the spots used for FFT filtering to yield the image in (F).

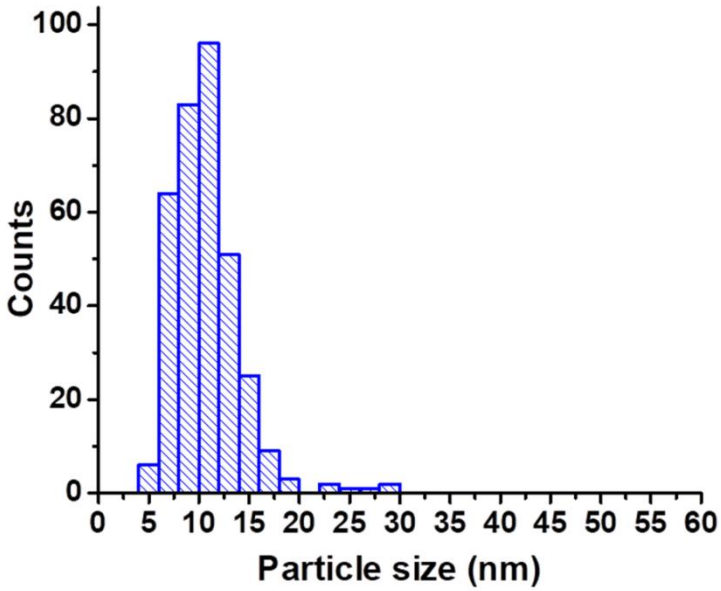

Fig. S3 Particle size distribution of o-Ni_2Si nanocrystals.

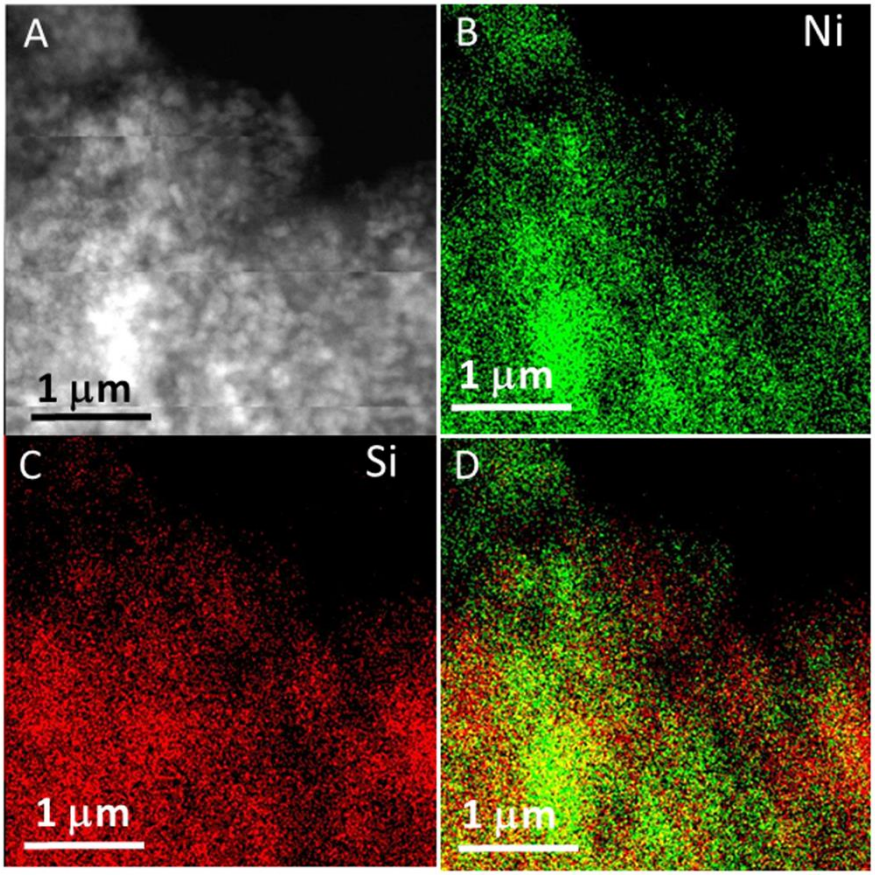

Fig. S4 (A) STEM-HAADF image and corresponding STEM-EDX mapping of o-Ni_2Si nanocrystals showing a homogenous distribution of (B) nickel (green), (C) silicon (red) and (D) Ni with Si.

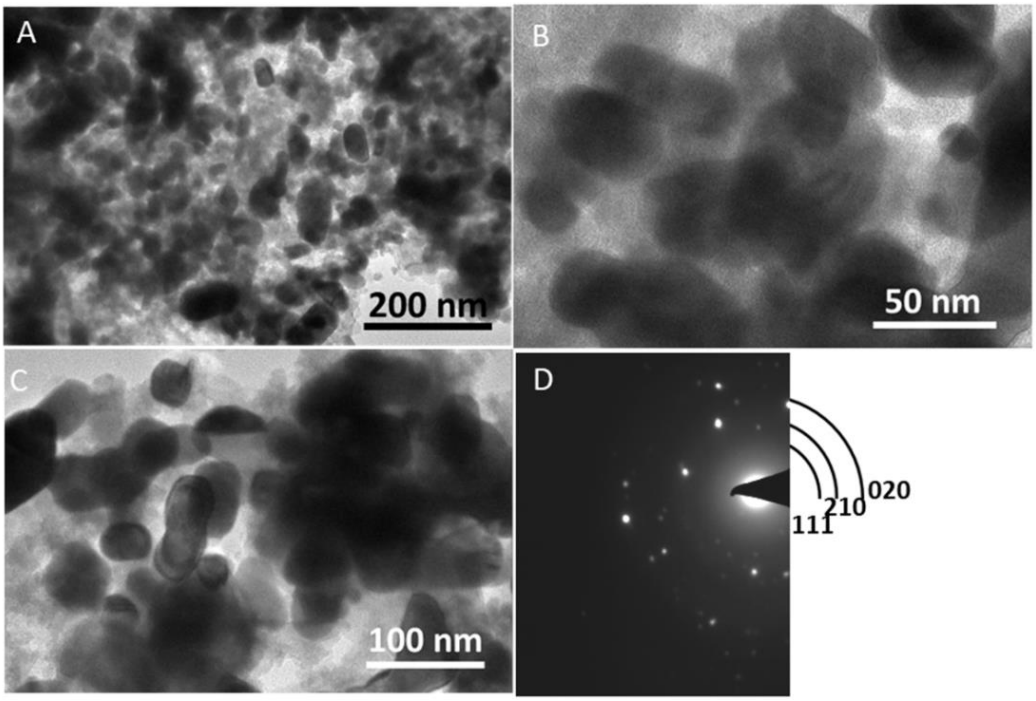

Fig. S5 TEM images and corresponding SAED pattern of NiSi nanocrystals.

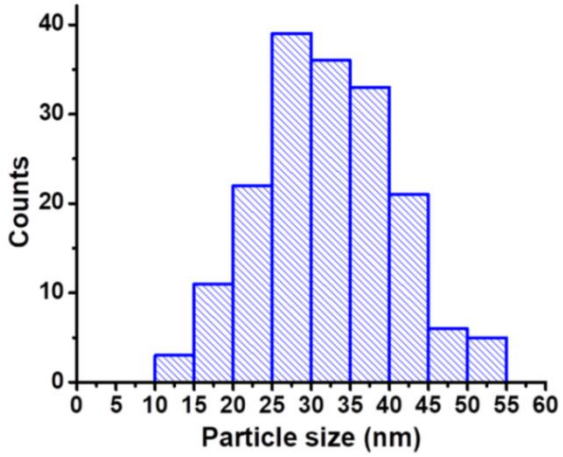

Fig. S6 Particle size distribution of NiSi nanocrystals.

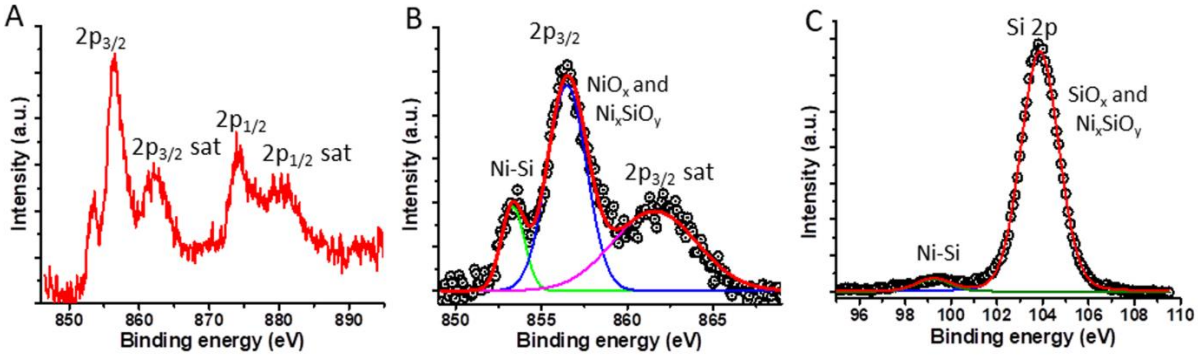

Fig. S7 (A, B) Ni $2p_{1/2}$ and $2p_{3/2}$, (B) Ni $2p_{3/2}$ fitted to different chemical environments and (C) Si 2p core level regions of XPS spectra of NiSi nanocrystals.

Table S1: XPS peak parameters of NiSi nanocrystals. The peaks are referenced with respect to the aliphatic C1s signal (284.8 eV).

Core level	Binding energy (eV)	Assignment
Ni $2p_{3/2}$	853.3	Intermetallic Ni-Si bond
Ni $2p_{3/2}$	856.5	Oxidized NiSi surface NiO_x and $NiSiO_x$
Ni $2p_{3/2}$ satellite	861.6	-
Ni $2p_{1/2}$	874.2	-
Ni $2p_{1/2}$ satellite	880.2	
Si 2p	99.2	Intermetallic Ni-Si bond
Si 2p	103.8	SiO_x and Ni_xSiO_y surface layer

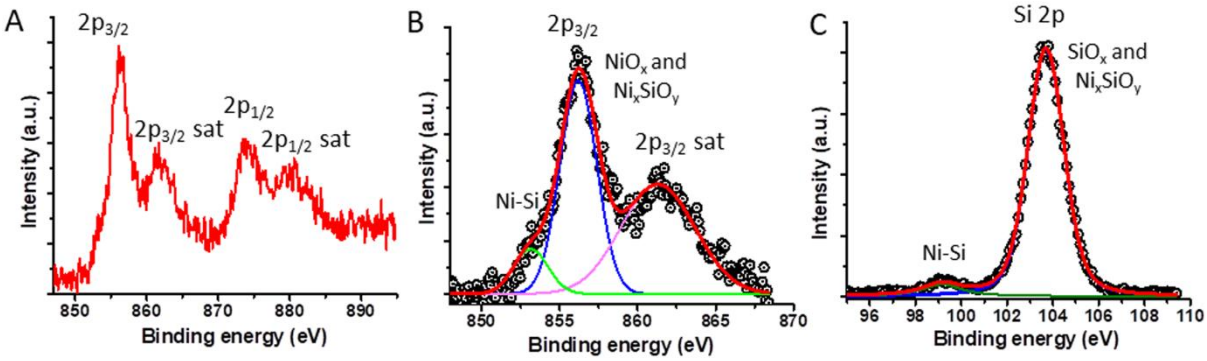

Fig. S8 (A, B) Ni $2p_{1/2}$ and $2p_{3/2}$, (B) Ni $2p_{3/2}$ fitted to different chemical environments (C) Si 2p core level regions of XPS spectra of o-Ni_2Si nanocrystals.

Table S2: XPS peak parameters of Ni_2Si nanocrystals. The peaks are referenced with respect to the aliphatic C1s signal (284.8 eV).

Core level	Binding energy (eV)	Assignment
Ni $2p_{3/2}$	853.1	Intermetallic Ni-Si bond
Ni $2p_{3/2}$	856.2	Oxidized Ni_2Si surface NiO_x and Ni_xSiO_y
Ni $2p_{3/2}$ satellite	861.3	-
Ni $2p_{1/2}$	844.2	-
Ni $2p_{1/2}$ satellite	880.2	-
Si 2p	99.2	Intermetallic Ni-Si bond
Si 2p	103.7	SiO_x and Ni_xSiO_y surface layer

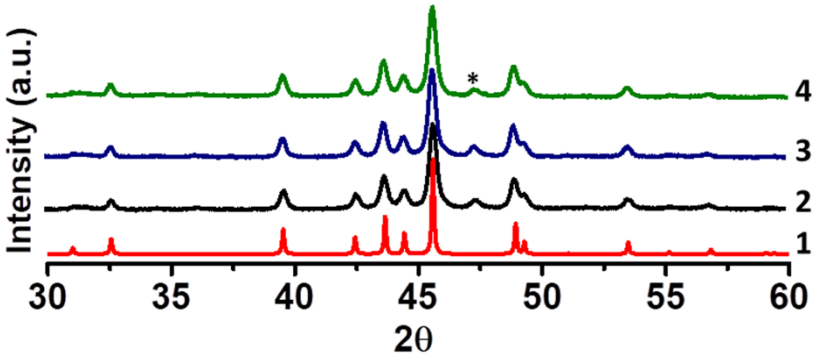

Fig. S9 Structural stability of Ni_2Si in different chemical environments. Powder XRD pattern of (1) simulated orthorhombic Ni_2Si, (2) pristine Ni_2Si, (3) in 0.1 M HCl solution for 12 h, (4) in 2 mol L^{-1} NaOH solution for 5 h. The asterisk corresponds to the Ni_2Si hexagonal polymorph.

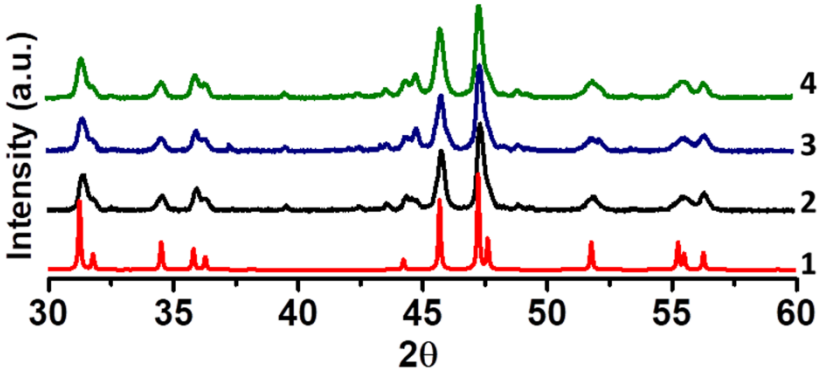

Fig. S10 Structural stability of NiSi in different chemical environments. XRD pattern of (1) simulated NiSi, (2) pristine NiSi, (3) in 0.1 M HCl solution for 12 h, (4) in 2 mol L^{-1} NaOH solution for 5 h.

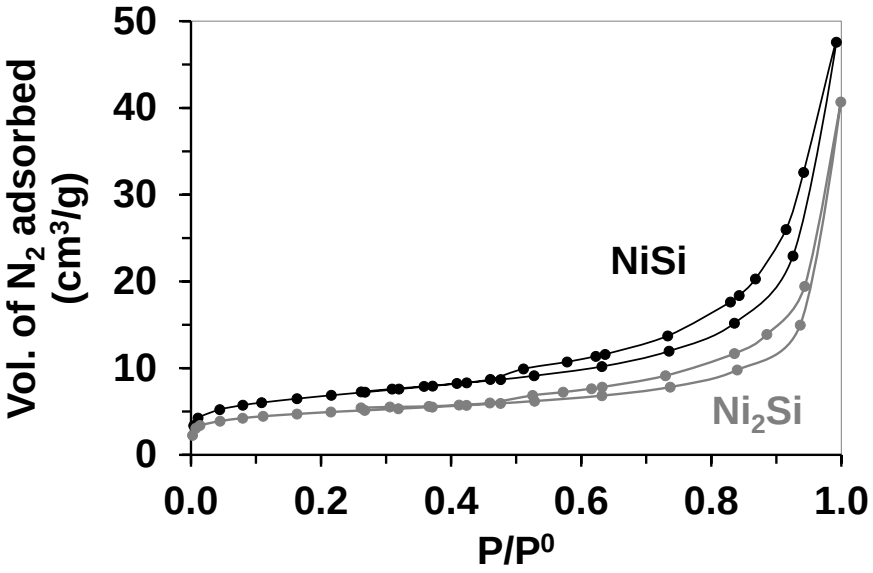

Fig. S11 Nitrogen adsorption-desorption isotherms of NiSi and o-Ni_2Si at 77 K.

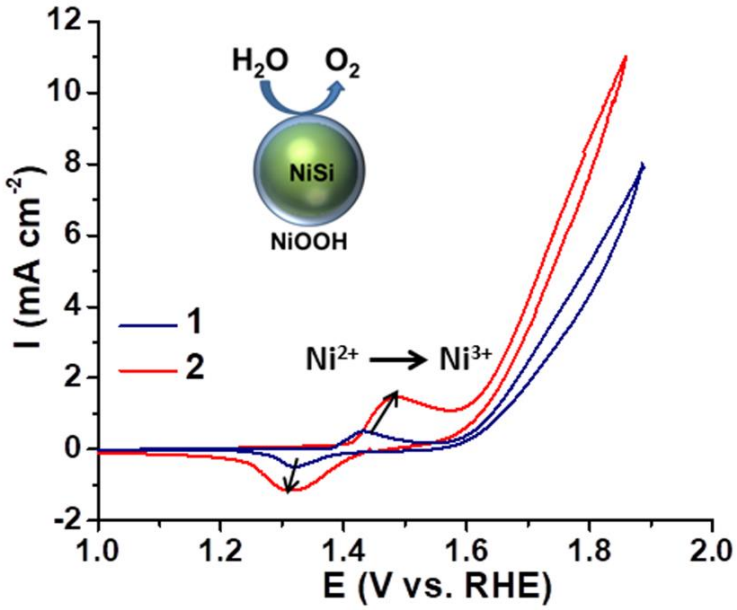

Fig. S12 Cyclic voltammograms (CVs) of NiSi before (1 blue) and after (2 red) 17 h chronopotentiometry stability test with a scan rate of 10 mV s^{-1} in O_2-saturated 0.1 M KOH on a disk electrode rotating at 1600 rpm. The potential was corrected for iR_s drop. The CVs show an increase in the $Ni^{2+} \rightarrow Ni^{3+}$ area due to the formation of electrochemically active NiOOH at the surface of the particles. The OER current density increases at the same time as surface oxidation activates the material.

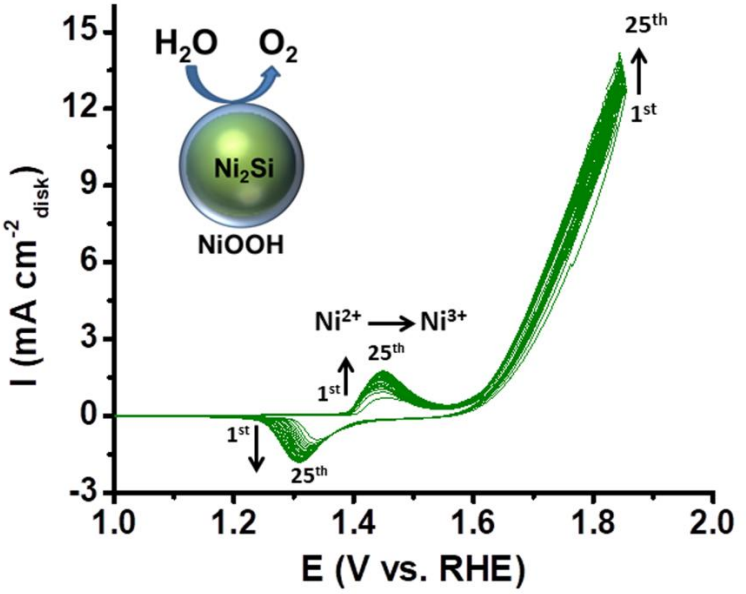

Fig. S13 Cyclic voltammograms (CVs) of o-Ni_2Si (first 25 cycles) with a scan rate of 10 mV s^{-1} in O_2-saturated 0.1 M KOH on a disk electrode rotating at 1600 rpm. The potential was corrected for iR_s drop. The CVs show an increase in the $Ni^{2+} \rightarrow Ni^{3+}$ area due to the formation of electrochemically active NiOOH at the surface of the particles. The OER current density increases at the same time as surface oxidation activates the material.

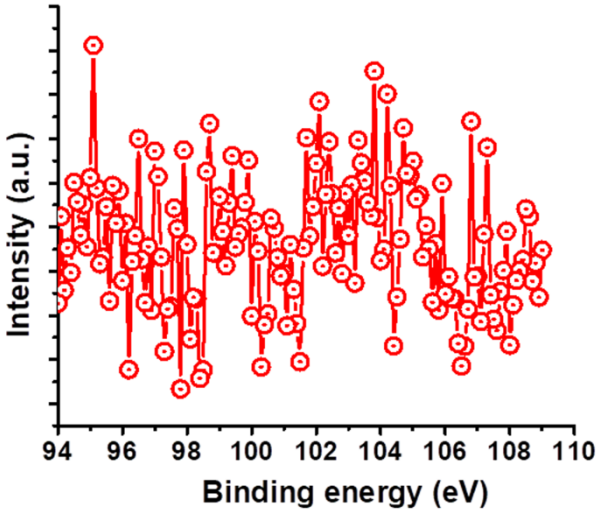

Fig. S14 Si 2p core level region of NiSi electrode after 17 h chronopotentiometry at 5 mA cm^{-2}disk.

Table S3: Nickel-p-block element compounds as OER electrocatalysts. Comparison of some key values from the literature.

Material	Reference	Measurement condition	Catalyst loading ($\mu g\ cm^{-2}_{disk}$)	I at 1.7 V/RHE ($mA\ cm^{-2}_{disk}$)	Mass activity: Catalyst mass-normalized current at 1.7 V/RHE ($mA\ .\ mg^{-1}$)	Mole activity: Current normalized to Ni content at 1.7 V/RHE ($A\ .\ mmol\ of\ Ni^{-1}$)
NiSi Ni_2Si	**Present work**	**0.1 M KOH, glassy carbon, 3 electrode**	**40**	**4.8 (NiSi) 5.0 (Ni_2Si)**	**120, 125**	**10.4, 9.1**
Ni_3Se_4	4	0.1 M KOH, carbon paper	500	60	120	19.7
$Cu_{2-x}Se/Ni_3Se_4$	4	0.1 M KOH, carbon paper	500	100	200	
Ni_xB	5	1M KOH, glassy carbon electrode	210	30	143	-
Ni_3B	6	1M KOH, glassy carbon electrode	300	20	67	4.2
Ni_3Se_2	7	0.3 M KOH, Au coated glass substrate electrode	435	32	74	8.2
Ni_3N/Ni foam	8	1M KOH, Ni foam support electrode	-	60	-	-
Ni_2P	9	1M KOH, Ni foam support electrode	5000	30	6	0.45

References:

1 A. Courac, Y. Le Godec, C. Renero-Lecuna, H. Moutaabbid, R. Kumar, C. Coelho-Diogo, C. Gervais and D. Portehault, *Inorg. Chem.*, 2019, **58**, 10822–10828.

2 X. Ma, F. Xu, T. M. Atkins, A. M. Goforth, D. Neiner, A. Navrotsky and S. M. Kauzlarich, *Dalt. Trans.*, 2009, 10250–10255.

3 J. Suntivich, H. A. Gasteiger, N. Yabuuchi and Y. Shao-Horn, *J. Electrochem. Soc.*, 2010, **157**, B1263.

4 S. Kim, H. Mizuno, M. Saruyama, M. Sakamoto, M. Haruta, H. Kurata, T. Yamada, K. Domen and T. Teranishi, *Chem. Sci.*, 2020, **11**, 1523–1530.

5 J. Masa, I. Sinev, H. Mistry, E. Ventosa, M. de la Mata, J. Arbiol, M. Muhler, B. Roldan Cuenya and W. Schuhmann, *Adv. Energy Mater.*, 2017, **7**, 1700381.

6 W.-J. Jiang, S. Niu, T. Tang, Q.-H. Zhang, X.-Z. Liu, Y. Zhang, Y.-Y. Chen, J.-H. Li, L. Gu, L.-J. Wan and J.-S. Hu, *Angew. Chemie Int. Ed.*, 2017, **56**, 6572–6577.

7 A. T. Swesi, J. Masud and M. Nath, *Energy Environ. Sci.*, 2016, **9**, 1771–1782.

8 M. Shalom, D. Ressnig, X. Yang, G. Clavel, T. P. Fellinger and M. Antonietti, *J. Mater. Chem. A*, 2015, **3**, 8171–8177.

9 L. A. Stern, L. Feng, F. Song and X. Hu, *Energy Environ. Sci.*, 2015, **8**, 2347–2351.